ADVANCES IN ATMOSPHERIC SCIENCES, VOL. 36, DECEMBER 2019, 1327–1339

• Original Paper •

Analysis of Determinants for an Enhanced and Long-lasting Coastal Convective System by Means of a Case Study (26 July 2011)

Jung-Tae LEE[1,2], Dong-In LEE[*2], Shingo SHIMIZU[3], and Cheol-Hwan YOU[2]

[1]*New and Renewable Energy Resource Center*, *Korea Institute of Energy Research*, *Daejeon* 34129, *Republic of Korea*

[2]*Department of Environmental Atmospheric Science*, *Pukyong National University*, *Busan* 48513, *Republic of Korea*

[3]*Storm*, *Flood*, *and Landslide Research Department*, *National Research Institute for Earth Science and Disaster Resilience*, *Tsukuba* 305-0006, *Japan*

(Received 3 February 2019; revised 30 June 2019; accepted 22 July 2019)

ABSTRACT

A precipitation system developed continuously along the western coastline of the Korean Peninsula and created considerable precipitation both along the coast and inland on 26 July 2011. In this study, the causes for this nearshore convective system are investigated from observations and the results of model experiments. Three-dimensional radar fields clearly show that a change of wind at the surface border played an important role in the development of the nearshore convection system. The simulation results, which are very similar to the observations, show that the surface border generated and maintained the convergence zone. The roughness change enhanced the convergence, and the interaction between the deepening cold pool and downward flow maintained the convergence zone. The surface mechanical discontinuity affected by the roughness change between sea and land formed the convergence (gradient of wind stress), which induced momentum transfer to the upper layer. The cold pool created a steep gradient of potential temperature and provided the reason for the propagated convergence zone with the downward flow. The maximum value of the surface change factor, which comprises the influencing factors for the long-lasting convective system, reflects the enhancement of the system at the coast.

Key words: coastal precipitation, roughness, convergence zone, cold pool propagation, downward flow

Citation: Lee, J.-T., D.-I. Lee, S. Shimizu, and C.-H. You, 2019: Analysis of determinants for an enhanced and long-lasting coastal convective system by means of a case study (26 July 2011). *Adv. Atmos. Sci.*, **36**(12), 1327–1339, https://doi.org/10.1007/s00376-019-9025-x.

Article Highlights:

- Three-dimensional radar fields clearly show that a change of wind at the surface border played an important role in the development of the nearshore convection system.
- This study suggests that steep gradient of wind stress and potential temperature can be major factors in the formation of the discontinuity and that the well-formed cold pool and downward flow are responsible for maintaining convergence.
- Surface change factor, which includes determinants for coastal precipitation (CP) is sufficient for representing and diagnosing the development of CP.

1. Introduction

The meteorological phenomena that occur in coastal areas can be summarized as sea breezes, coastal fronts, coastal jets, typhoon landfalls and coastal precipitation (CP). A sea breeze is a local coastal wind that blows from the sea to the land and can cause convection near the coast (Mazón and Pino, 2013; Chen et al., 2015). A coastal jet is induced by mountain barrier and may cause rising air and heavy rainfall if it continues to develop (Christakos et al., 2014; Ke et al., 2019). The landfall of a typhoon is very well known and is the cause of much precipitation and damage in coastal areas (Gray et al., 1997; Woodruff et al., 2013). Because all these coastal phenomena have the potential to cause flash floods, they have been analyzed in various ways for a long time. CP, which refers to concentrated rainfall in a coastal inland area, is the result of various weather phenomena. Given that much of the world's population resides in coastal areas, CP has a significant impact on human activity. Although studies of the formation and mechanisms of CP have been conducted for a long time (Bergeron,

* Corresponding author: Dong-In LEE
Email: leedi@pknu.ac.kr

1949; Nyberg and Modén, 1966; Camberlin and Planchon, 1997; Braun et al., 1999; Attema and Lenderink, 2014), it has been difficult to elicit their causality because of the complex interrelationships among physical processes. Furthermore, since numerous studies have been focused on better boundary layer simulation, the mechanism of CP was far from being the main research subject. Therefore, CP remains incompletely understood, thereby justifying the present research.

The characteristics of CP are the precipitation maxima that appear inland. Bergeron (1949) first identified precipitation maxima in the coastal region of the Netherlands. Later, Nyberg and Modén (1966) found the precipitation distributions for Stockholm to be similar to the precipitation maxima of the Netherlands. In the past, a lack of scientific data caused technical limitations in identifying the cause of CP, but in recent years climate characteristics have been derived from a set of meteorological instruments and model data (Attema and Lenderink, 2014). According to climatological studies (Roxy et al., 2015; Drobinski et al., 2018; Yang et al., 2018), CP with morphological clearness is generally induced by sharp changes in the transfer of heat, moisture and momentum between land and sea. These sudden changes are due fundamentally to the differences in specific heat, roughness, radiation and boundary-layer conditions. These factors have long been thought to profoundly affect the precipitation processes in coastal areas, and indeed such factors can cause an unequilibrated state on the low-level flow and induce a transfer of energy to the upper side when the air moves inland from the sea (Persson et al., 2005). The process between land and sea could be a climatic feature in Korea, where the coastline stretches out towards the meridian and westerly winds are affected (Lee et al., 1998). Sun and Lee (2002) revealed that heat flux has a substantial influence on Korea's climatic features, and many studies have shown heat flux to be a major factor in convective development or explosive deepening (Langland et al., 1995; Gyakum and Danielson, 2000; Hirata et al., 2015). Furthermore, the sea–land roughness change can also sufficiently infer the possibility of convective development from studies of the growth of the atmospheric internal boundary layer and turbulence due to surface discontinuity (Wu, 1969, 1982; Oerlemans, 1980; Plant and Atkinson, 2002; Lee, 2015; Pires et al., 2015), although its mechanism is yet to be fully clarified.

Even though many studies of the surface processes in coastal regions have been conducted for decades, these phenomena (e.g., sea breezes, fog, extratropical cyclones and consequent CP) remain incompletely understood because they result from interactions in the total geophysical system (i.e., among air, sea and land). Furthermore, it is not easy to identify the mechanism, because a moving precipitation system can become stagnant because of various interactions when it experiences surface discontinuity. It means that the surface processes alone do not account for all the mechanisms of long-lasting precipitation. In addition, most previous studies focused on the contribution of heat flux to convection on the large scale (Ross et al., 2004; Sridhar, 2013; Gentine et al., 2016; Schlemmer and Hohenegger, 2016), whereas surface wind stress could be an important source that changes the air flow by forming turbulent flow. If the heat exchange between land and air is sufficiently weak, the mechanical process due to the increased wind stress becomes an important factor in the effect of the surface border. In particular, there is a need to study the development of CP associated with the roughness change in a coastal region that is orientated orthogonally to the main motion of the precipitation system, as is the case with the Korean Peninsula.

The present precipitation system case (26 July 2011), which occurred mainly in the Yellow Sea and resulted in a considerable amount of precipitation, was distributed at the coast. However, if new convective cells are generated near the coast (Lee et al., 2014), even more intense precipitation is often observed in the area. This distribution of precipitation on the Korean Peninsula causes us to speculate that many of the convective systems that develop in the Yellow Sea cause more precipitation because of interaction with the surface.

The aims of the present study are to (i) demonstrate the interaction between the developed precipitation system and the surface border and (ii) determine which processes and factors contribute to the development and maintenance of convection in the region near the shore of Gyeonggi Bay. To achieve those aims, a case study of heavy rainfall was conducted using observational data and model simulation. The main factors for nearshore enhanced precipitation revealed by the analysis were verified through numerical experiments.

2. Data and methods

2.1. *Observation data*

In this study, ground-based S-band Doppler radars (KWK, GDK, IIA) operated by the Korea Meteorological Administration (KMA) were used to retrieve three-dimensional wind fields (Fig. 1). To avoid errors in the remotely sensed data, non-meteorological targets (birds, sea clutter and other unreasonable values) were eliminated using the method proposed by Zhang et al. (2004). The preprocessed radar data were interpolated to a Cartesian grid using the interpolation scheme proposed by Cressman (1959). The intervals of the horizontal and vertical grids were 1 and 0.25 km, respectively, with effective radii of 1.5 and 1.0 km, respectively. The amount of surface rainfall was recorded by the Automatic Weather System (AWS) of the KMA. The spatial distribution of rainfall is shown as the observation through a minimum curvature method (Smith and Wessel, 1990).

2.2. *Wind-field synthesis*

Using variational-based wind analysis to treat the problem involved in the specification of the boundary condition between the top and bottom level has advantages for retriev-

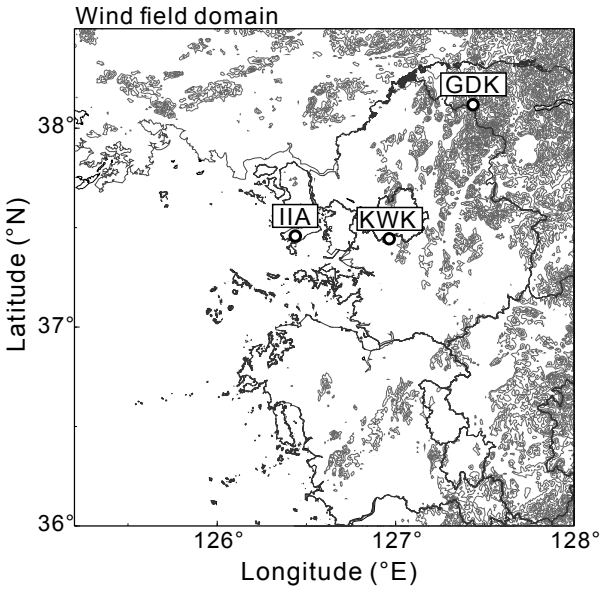

Fig. 1. Domain of retrieved wind field (Gyeonggi Bay). The circles show radar sites operated by the KMA. The topography is contoured in 100-m intervals (thin gray line).

ing the appropriate vertical velocity (Liou and Chang, 2009). Moreover, Liou et al. (2012) suggested advanced radar wind synthesis of the three-dimensional wind field on a non-flat surface, and it was implemented without conversion to the terrain-following coordinate system by using the immersed boundary method (Tseng and Ferziger, 2003). Consequently, we created three-dimensional wind-field data using an algorithm designed by Liou et al. (2012), named WISSDOM (Wind Synthesis System using Doppler Measurement). It can estimate reasonable horizontal and vertical wind patterns considering terrain forcing, which is suitable for the wind field along the baseline, courtesy of resolving the anelastic continuity equation and the simplified vertical vorticity equation.

2.3. *Simulation*

The configuration of the Cloud-Resolving Storm Simulator (CReSS; Tsuboki and Sakakibara, 2002) V3.4 is given in Table 1. CReSS is based on the non-hydrostatic and compressible equation. The prognostic equation solves for the following five variables: (i) vector (u, v and w), (ii) perturbation of pressure, (iii) perturbation of potential temperature, (iv) mixing ratio (six categories) and (v) turbulent kinetic energy (TKE). The microphysics parameterization scheme is implemented by the bulk method of cold rain suggested by Lin et al. (1983), Ikawa and Saito (1991) and Murakami et al. (1994). This bulk scheme covers six types of hydrometeor—namely, water vapor, rain, cloud, ice, snow and graupel.

The parameterization scheme for the surface boundary layer (SBL) is that suggested by Segami et al. (1989). CReSS simulates physical processes in the SBL for a shorter integration time than those of other well-known cloud resolving models (RAMS and ARPS), and is therefore appropriate for analyzing changes in the SBL. The potential temperature flux (θ_{flux}) used in the present study is vertically constant in the SBL and is expressed on the basis of the mixing-length theory of Prandtl (1925) as

$$\theta_{\text{flux}} = \frac{H_{\text{flux}}}{\rho C_p} = -C_{\text{h}}\left(\bar{\theta} - \theta_{\text{G}}\right)\bar{u}\,, \tag{1}$$

where H_{flux} (J m^{-2} s^{-1}) is the sensible heat flux, ρ is the air density (kg m^{-3}) and C_p is the specific heat (1,004 J K kg^{-1}). On the right-hand side of Eq. (1), C_{h} is the bulk coefficient of sensible heat and potential temperature (non-dimensional; Louis et al., 1982) and is formed by the roughness length Z_0, which follows the Global Land Cover Characterization (GLCC) data for each type of surface (Table 2). The difference $\left(\bar{\theta} - \theta_{\text{G}}\right)$ is the difference in θ between the SBL and the ground, and $\bar{u}$ is the mean zonal wind component of the SBL. The Reynolds stress to express surface momentum energy is given as

$$\tau_{\text{Reynolds}} = \left[\tau_{zx}^2 + \tau_{zy}^2\right]^{\frac{1}{2}}\,, \tag{2}$$

where τ_{zx} and τ_{zy} are the horizontal shear stress in the zonal and meridional direction, respectively.

We used the CReSS model to simulate the convective sys-

Table 1. Model configuration in CReSS.

Feature	Configuration
Initial/boundary condition	MSM forecast (3 h)
Projection	Lambert conformal
Grid	Arakawa C-type
Microphysics	Bulk cold rain with mass
Top/bottom boundary conditions	Rigid boundary
Sponge layer	Above 14 km AGL
Horizontal/vertical advection	Forth-order/second-order scheme
Time splitting	HE-VI
Advection scheme	Forth-order scheme (horizontal)
Turbulent parameterization	1.5-order turbulence closure
Surface processes	Energy/momentum fluxes

Table 2. Land description and surface constant (GLCC).

Description	Albedo	$Z_{0,m}$	$Z_{0,h}$	Evapotranspiration efficiency
Water bodies	0.06	2.4×10^{-4}	2.4×10^{-4}	1.0
Urban and built-up land	0.25	0.5	0.1	0.05
Dry cropland and pasture	0.2	0.12	0.1	0.15
Irrigated cropland and pasture	0.1	0.075	0.1	0.6
Mixed dry/irrigated cropland and pasture	0.2	0.5	0.1	0.3
Cropland/grassland mosaic	0.2	0.4	0.1	0.5
Cropland/woodland mosaic	0.2	0.4	0.1	0.5

tem from 0900 LST 26 July 2011 to 0600 LST 27 July 2011. The simulation domain is shown in Fig. 2. The mesoscale model (MSM) that is produced every 3 h by the Japan Meteorological Agency was used as the initial condition (0900 LST 26 July 2011). The control (CTL) and no-land (NL) experiments were nested to a 1-km grid from the D1 to D2 (2 km) domains. The experiments with 1-km resolution had a large time step of 2 s, contained 81 vertical levels and had a high resolution of 100 m below 1.5 km above the surface layer (ASL). To clarify the influence of surface discontinuity, we compared CTL with NL. The NL experiment was conducted by replacing the land region of the Korean Peninsula (below 38°N) with sea. Such an experiment with change in land cover is suitable for analyzing the impact of surface discontinuity (Baidya Roy and Avissar, 2002; Pielke Sr et al., 2007). The NL and CTL experiments both used the average MGDSST (Merged satellite and in-situ data Global Daily Sea Surface Temperature) of the Yellow Sea on 26 July 2011. In order to investigate the impact of surface discontinuity only, the NL experiment used the same topography as CTL.

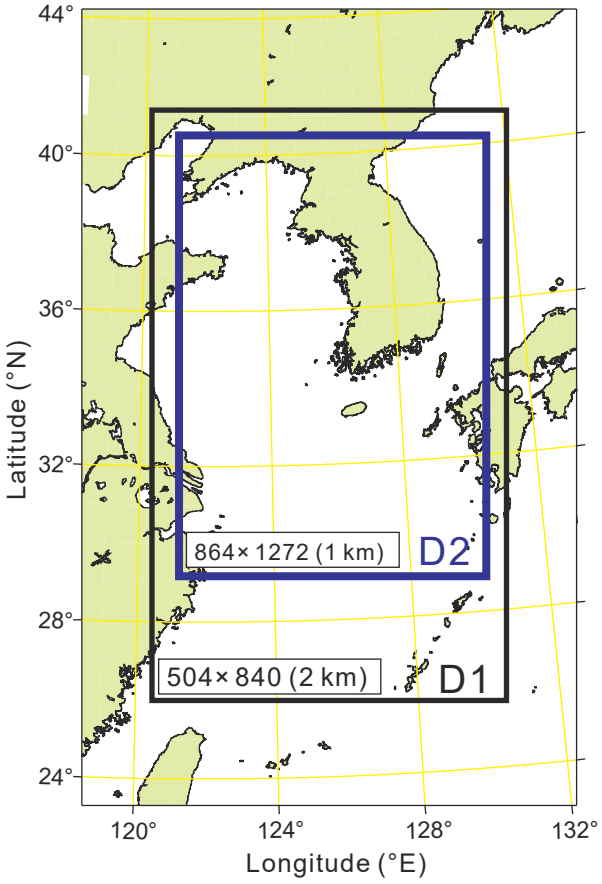

Fig. 2. Domains for experiments. D2 (1 km) is nested into D1 (2 km).

2.4. *Quantification of coastal processes*

To quantify the processes that increase the precipitation in coastal regions, we used vertically integrated factors within effective layers. The factors considered were those parameters (i.e., turbulent flux, water vapor, TKE and potential temperature perturbation) that are recognized as substantial elements for nearshore precipitation. The formulas for the vertically integrated water-vapor turbulent flux (IWF) and the surface change factor (SCF) are

$$\mathrm{IWF} = \int_{Z_1}^{Z_2} \frac{1}{g} q_v \left(\boldsymbol{V} - \overline{\boldsymbol{V}} \right), \tag{3}$$

$$\mathrm{SCF} = \int_{Z_1}^{Z_2} -\nabla \left[\theta' \mathrm{TKE} \left(\boldsymbol{V} - \overline{\boldsymbol{V}} \right) \right] \mathrm{d}z, \tag{4}$$

$$\boldsymbol{V} = \boldsymbol{u} + \boldsymbol{v}, \tag{5}$$

where $\boldsymbol{V}$ is the horizontal atmospheric motion vector, $\overline{\boldsymbol{V}}$ is the spatial mean of the horizontal atmospheric motion, q_v is the water vapor (kg m^{-3}), g is the gravitational acceleration (m s^{-2}), Z_1 is the lowest level of the air (SBL level; 50 m) and Z_2 is the maximum height at which the TKE reacts and energy transfer is possible in the lower layer (2000 m).

3. Results

3.1. *Case overview*

The rainfall case of 26 July 2011 caused over 150 mm of accumulated rainfall over 9 h (1500 LST 26 July 2011 to 0000 LST 27 July 2011) over the middle of the Korean Peninsula. The precipitation continued until the afternoon of 27 July, and flash floods and landslides occurred in the Seoul metropolitan area. Lee et al. (2014) conducted a synoptic analysis of the case. The potentially unstable environment due to (i) the lower wet-air inflow from the southwest of the Korean Peninsula and (ii) the middle-level drying from the

northwest of the Korean Peninsula created a favorable environment for developing a quasi-stationary convective system with a trough that stretched from the northwest to the Korean Peninsula (Fig. 3). This case has been used widely in radar quantitative precipitation estimation and studies involving dynamical analysis (Jang and Hong, 2014; Jang et al., 2016; Lee et al., 2017) because of the unusually large amount of precipitation over the following four days (i.e., 26–29 July). There were various singularities, and the fact that the precipitation system on 26 July developed with the shape of the shoreline is appropriate for studying how surface processes affect precipitation development.

The precipitation system that initially occurred on 26 July shifted inland from the western ocean of Korea (Fig. 4a). The system, which moved from the west to the east, stayed on the coastline of Gyeonggi Bay and new cells continually developed along the coast. The precipitation system that was moving stayed in the coastal region (Fig. 4), causing analysts to assume that any difference between the sea and the land had affected the persistent development of the nearshore convection. The systems were long-lived and recorded area-weighted rainfall in the coastal region, making investigating the mechanism causing such CP worthwhile.

Various natural processes could have induced the area-weighted rainfall, but usually they can be summarized by certain thermal and mechanical processes. In Fig. 4f, the results regarding the processes involved are shown as a system-relative wind vector inland. The precipitation systems moved towards the northeast. However, the wind vectors over the land were oriented in the opposite direction to that

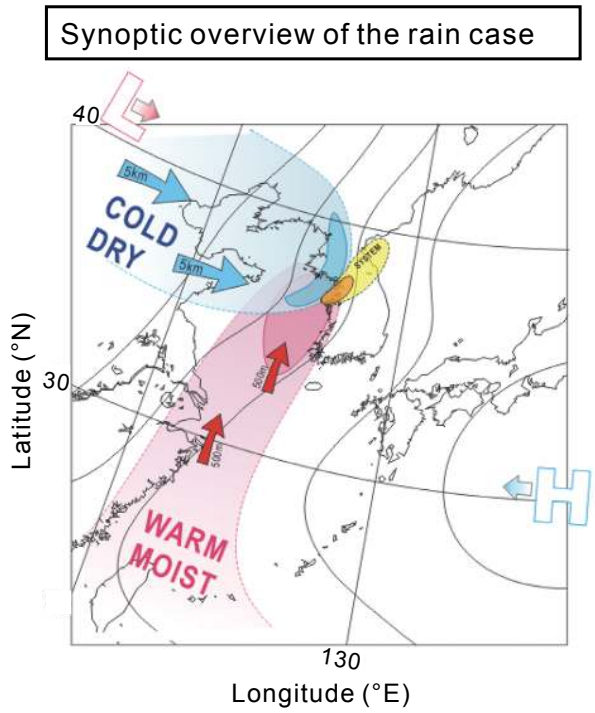

Fig. 3. Schematic diagram of a synoptic mechanism for heavy rainfall on 26 July 2011. The solid contours are the isobars representing the trough.

in which the system moved, which means that there was a force blocking the inflow of air. This force seems to have been a mechanical process that occurred over the surface discontinuity, because the temperature difference between sea and land was small (less than 2°C). We therefore deemed it to be a reason for the long-lasting CP. As shown by Lee et al. (2014), surface-roughness change is a substantial factor for decreased wind speed. It decreases the wind speed at the boundary layer, which could have caused the low-level convergence shown in the 20–40-km range of line A–A' (1400–1600 LST; Fig. 4f). In other words, in the system relative wind (Fig. 4f; vectors), decreased wind speed is shown as arrows pointing in the opposite direction to that in which the system is moving. These vectors stand out near the surface border between sea and land. Consequently, the force that caused the wind vectors to point in the opposite direction to that in which the system is moving can be taken as being decreased wind speed due to surface-roughness discontinuity. Such decreased wind would have generated convergence and contributed to the development of CP. In addition, because the inland region of Gyeonggi Bay is flat, the forced convergence by the terrain does not need to be considered.

Considering previous studies and the positions of the opposing vectors, one can conclude that roughness discontinuity contributed much to the formation of the vectors. However, it would be inappropriate to jump to the conclusion that roughness discontinuity was the sole cause of all the opposing vectors in the relative wind speed because the magnitude of the force blocking the inflow varied (Fig. 4f). Generally, friction reduces wind speed by only 20% at the surface, but the vectors over the land were of varying magnitude and indicated a percentage that was sometimes greater than and sometimes less than 20%. In other words, the vectors most likely reflect additional forces that arose from other physical processes. Consequently, postulating roughness change as the sole reason is not a persuasive argument for the extent of the opposing vectors and long-lasting CP. Another factor to consider is the internal thermal boundary layer caused by the temperature difference between sea and land, but there was no significant temperature difference in the present case. One can consider various factors regarding the force that maintained the CP, but observations to date are unfortunately insufficient for exploring various scientific possibilities in more detail. Therefore, we examined the development of the CP by means of simulation in this study, which allowed for a more detailed analysis and to show the effect of the surface discontinuity.

3.2. *Coastal precipitation*

The CReSS model simulated the convective system on 26 July fairly well. To validate the simulation results, we compared the simulated accumulated rainfall and cloud pattern with observations (ground-based radars and AWS).

The distribution of simulated rainfall for 9 h in the central region of Korea was quite similar to the surface observa-

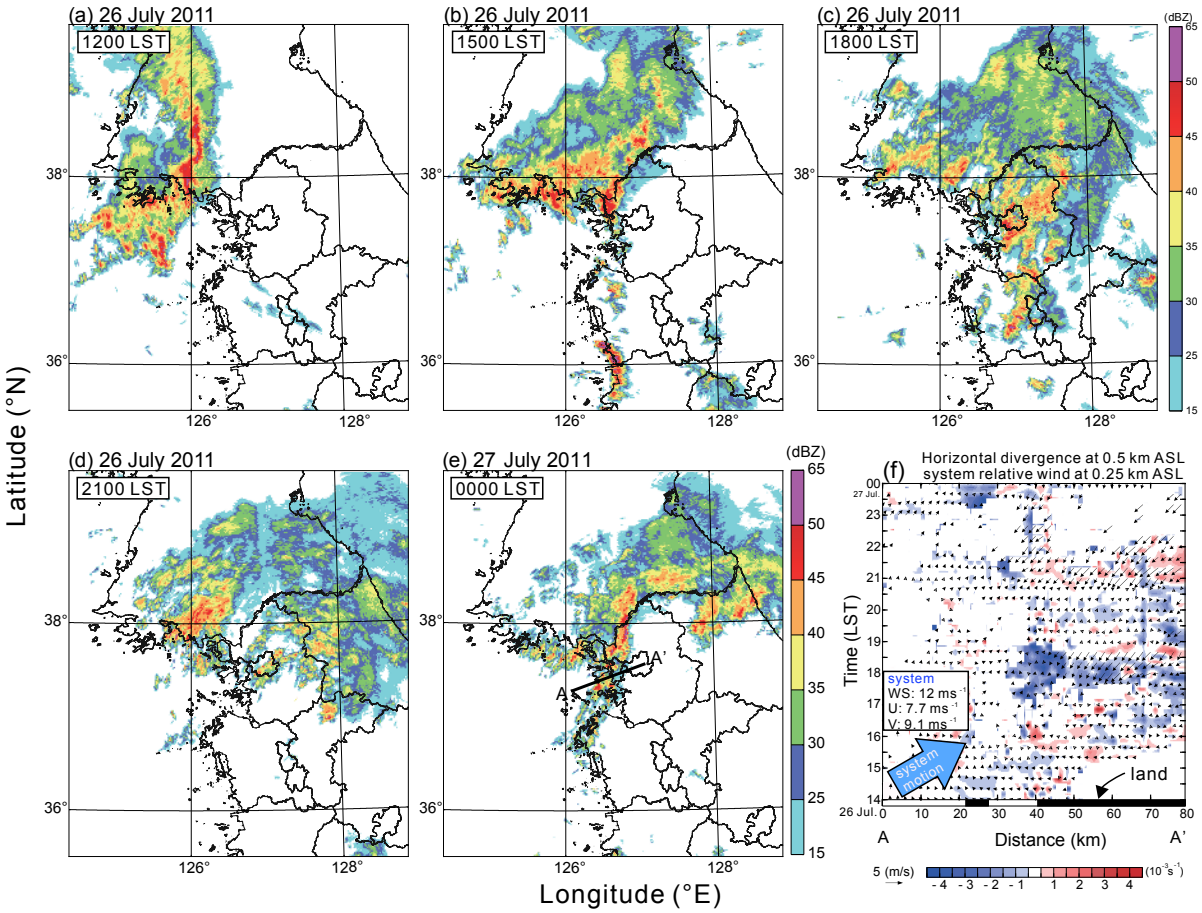

Fig. 4. Composited radar reflectivity at 1.5 km ASL at (a) 1200 LST (b) 1500 LST (c) 1800 LST (d) 2100 LST 26 July, and (e) 0000 LST 27 July. (f) Hovmöller diagram of horizontal divergence and system-relative wind vector at 0.5 km ASL along the line A–A' (black bars indicate onshore region). The system moving speed is 12 m s^{-1}.

tions (Fig. 5a). According to ground observation, the rainfall in excess of 150 mm was elongated in the east–west direction in the central region, and that in excess of 200 mm was shifted towards the west coast. The simulated rainfall in excess of 150 mm was located more in the south compared with the observations, but the model simulated shifted rainfall on the west coast. The accumulated rainfall of the model tended to be overestimated, but the rainfall distribution was quite similar to the surface observations. In particular, the model best described the cloud formed and convergence pattern (Fig. 4f) nearshore region compared with radar observation. Therefore, the model results were considered as representative and were used to reveal how the discontinuity of the surface condition induced CP.

Figure 6 shows the accumulated rainfall of NL and the difference in rainfall between CTL and NL (1500 LST 26 July–0000 LST 27 July). Positive differences in precipitation were distributed widely around Gyeonggi Bay; in particular, more than 250 mm was around the coast (Fig. 6b). Because the NL experiment was conducted under the assumption that the land was actually sea, there was a large difference in precipitation between the sea and the land. This difference shows that the 26 July case was sensitive to the surface discontinuity. NL simulated a small quantity of rainfall and could not form a precipitation system at the coast as much as CTL (Fig. 6a). There are various reasons why the model cannot create clouds, but the results of the experiments show that surface discontinuity was a major factor in the present case. The physical factors due to surface discontinuity include roughness, evapotranspiration, albedo and heat capacity, and differences in those factors affect the air flow in the lower layer, generally leading to a change in wind speed and temperature. The model uses a roughness length to simulate the process by which the surface features influence the wind pattern of the boundary layer. The thermal characteristics of the surface are $Z_{0,h}$ (roughness length for scalar) and momentum is $Z_{0,m}$ (roughness length for velocity). Figure 7 shows which of the two (momentum or heat) contributed more to forming surface differences. The mean spatial variation (line B–B') of the θ flux was about zero at sea but changed inland with a small fluctuation. The changes are clearly distinguishable from the sea to the land, but even inland they are not very large. It indicates that the transfer of thermal energy from the land to the air is inactive. If the land has sufficient thermal energy and transfer to the air is active, then a thermal IBL (Internal Boundary Layer) may form, but that situation does not pertain in the present case. It is similar to the NL simulation as-

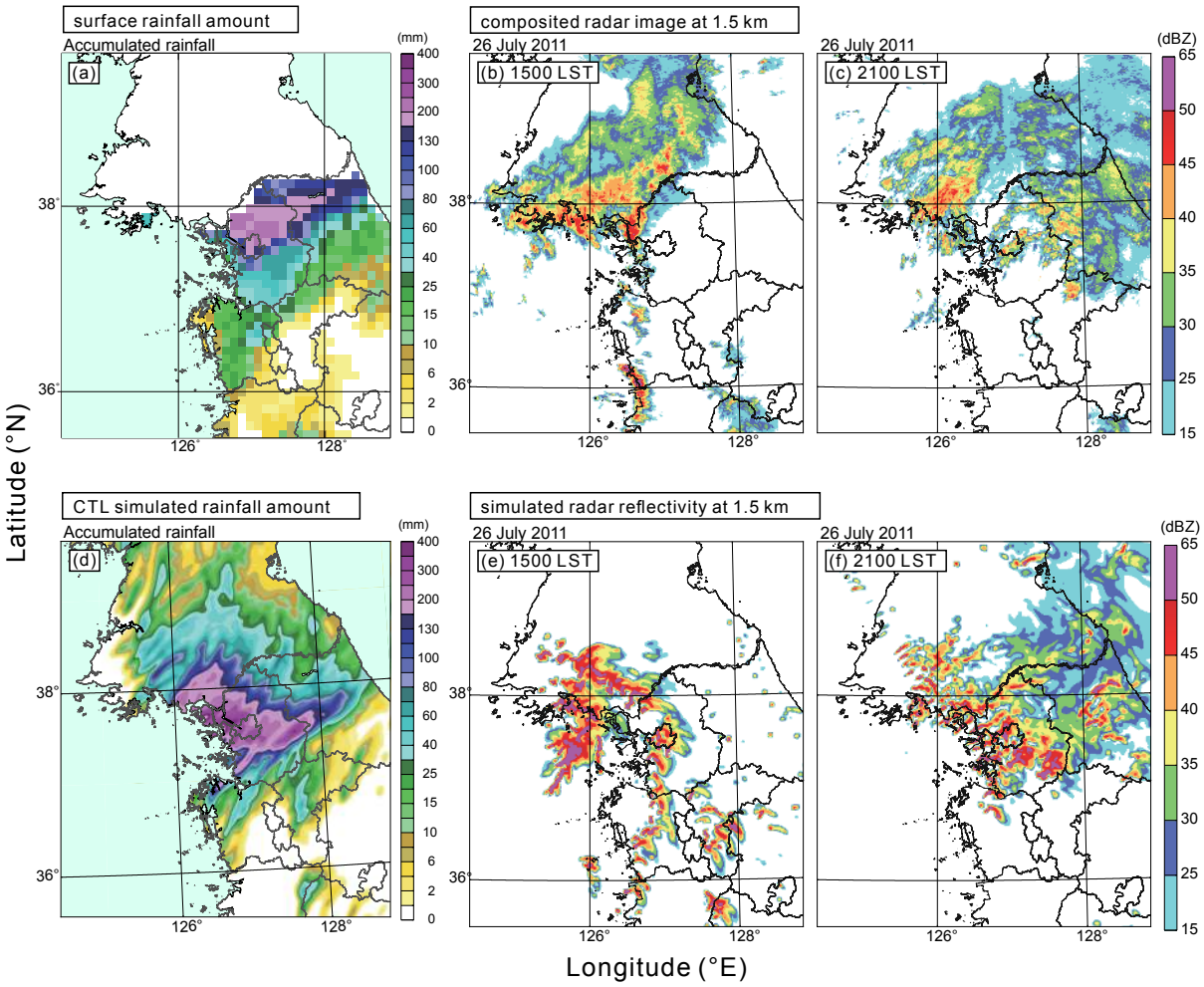

Fig. 5. Comparison of observation and CTL simulation: (a) observed accumulated rainfall for 9 h (1500 LST 26 to 0000 LST 27 July 2011); (d) CTL simulated rainfall for the same times as in the observation; (b, c) composited radar reflectivity at 1.5 km ASL; (e, f) simulated radar reflectivity of CTL experiment.

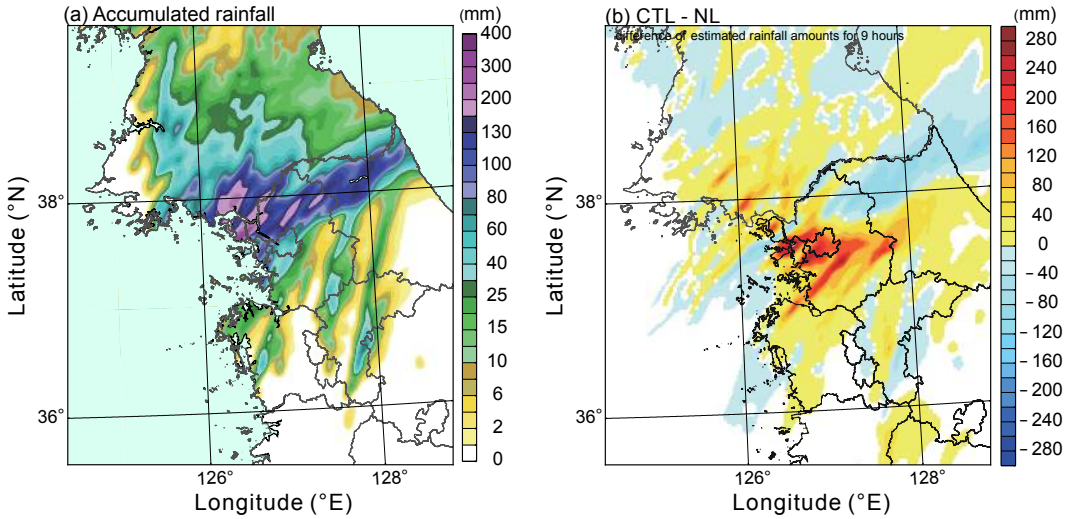

Fig. 6. (a) Accumulated rainfall of the NL experiment. (b) Difference in estimated rainfall amount for 9 h (1500 LST 26 to 0000 LST 27 July 2011) between the CTL and NL experiments.

suming land as the sea, and the exchange of θ_{flux} in NL was minor as in the sea area of CTL. By contrast, the Reynolds stress varies greatly from the sea to the land. Its value exceeded 0.4 over the land and showed a sudden increase at

the surface border (Fig. 7a). The distribution of Reynolds is stress shown in Fig. 7b. The values of 0.6–1.0 N m^{-2} are distributed inland along the coastline, and its maximum is about 1.4 N m^{-2} where precipitation occurs. The spatial variation of two surface variables indicates high levels of mechanical energy but relatively little thermal exchange. In other words, the mechanical process was dominant for the surface-wind decrease in the present case. The stress normally increases with the wind speed and air density, and the high stress in the present case was natural because there was a low-level jet at the 850-hPa height (Lee et al., 2014). The CReSS model has an algorithm that spreads the stress energy from the lower layer to the upper layer by applying a diffusion coefficient, which is assumed to have affected the development of convergence near the surface border.

However, the effect of the roughness change is not enough to explain the large difference in the amount of precipitation and long-lasting systems as mentioned before. Although the surface stress reduced the wind speed in the lower layer and the energy was transported to the upper layer, those processes are insufficient to account for the differences in precipitation (CTL minus NL). This claim is supported by the sustained and propagated convergence zone.

Figure 8 shows the horizontal divergence distribution and Hovmöller diagram for line C–C'. As seen in the horizontal distribution (Fig. 8a), convergence (blue) at low levels appeared along the coast. In the early stage of the precipitation system (1400–1500 LST), the convergence appeared inland. Strong low-level convergence ultimately contributes to convection, especially in the case of precipita-

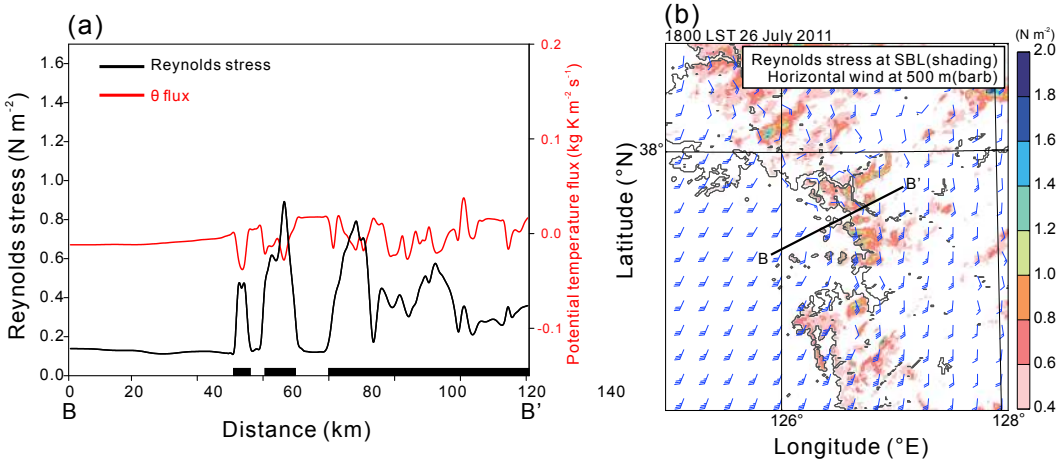

Fig. 7. (a) Mean spatial variation of surface parameters (Reynolds stress, potential temperature flux) for 10 h (1400 LST 26 to 0000 LST 27 July 2011). The horizontal black bars indicate onshore region. (b) Horizontal distribution of wind stress at the surface (shading) and wind barbs at 500 m ASL.

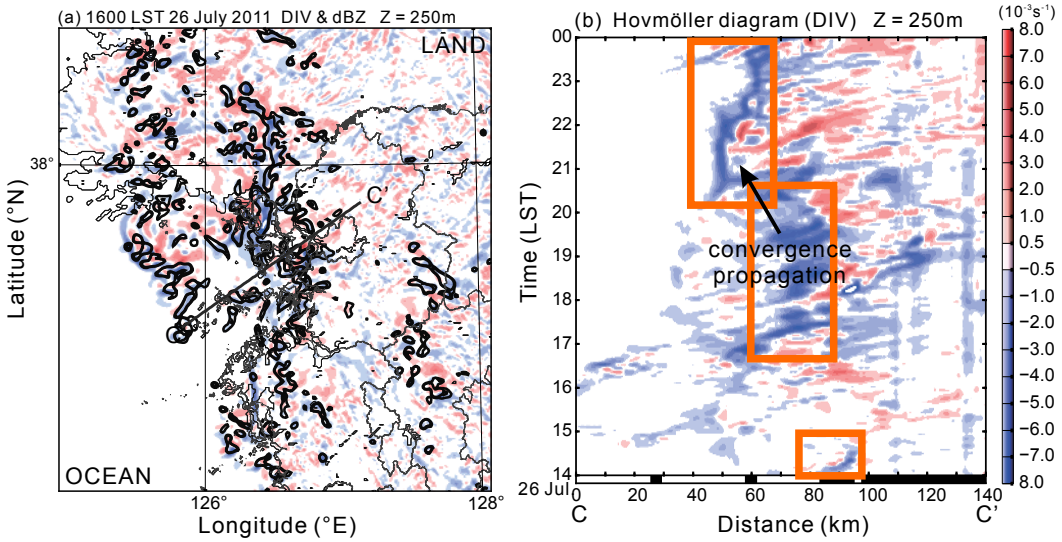

Fig. 8. (a) Divergence distribution and (b) Hovmöller diagram of CTL. The contours indicate the simulated precipitation system. The boxes (orange) indicate the region of convergence. The Hovmöller diagram is shown along transect C–C'.

tion. When a precipitation system makes landfall, it undergoes a change in velocity, and momentum transfer occurs vertically. This physical process is confirmed by the convergence near the coast. After that, the convergence was intensified near 1800 LST and shifted offshore. Its behavior is also remarkable in the observational results (Fig. 4f). It cannot be fully explained by the roughness change. In other words, other elements contributed to the sustainable convergence.

3.3. *Elements for sustainable convergence zone*

As mentioned before (section 3.2), the effect of surface discontinuity is insufficient to clarify the mechanism of CP, although roughness change contributes to the convergence. To describe the sustainable convergence zone, other physical elements are needed. The transect along line C–C' shown in Fig. 8 reveals which elements were substantial. Figure 9 shows the vertical structure of the precipitation system. A remarkable negative potential temperature perturbation (θ') is visible at low levels (shading in Fig. 9a). The negative θ' is due to evaporation cooling by precipitation and is generally described as a cold pool. When the cold pool develops properly, it forms a horizontal discontinuity of θ over 3 K that can generate upward flow at the border. The horizontal gradient of $\theta(\partial\theta/\partial xy)$ is about 1.7 K km^{-1} at the cold pool boundary, which shows a well-formed cold pool (de Szoeke et al., 2017). The low heat flux exchange (Fig. 7) with the land surface suggests the favorable condition under which the cold pool can mature. The upward flow at the border of the cold pool is also remarkable at 60 km of line B–B'. The vertical velocity exceeds 4 m s^{-1} and is sufficient to induce convective precipitation. This cold pool stayed near the coast and gradually propagated offshore. The propagation of the mature cold pool in the windward direction is a feature of a convective system accompanied by heavy rain (Li and Carbone, 2015; Jeong et al., 2016). Furthermore, the propagation occurred with the downward flow of the convective system. Such downward flow, which is a structural feature of a convective system, is produced in theory by falling precipitation. The descending flow is dispersed near the surface, thereby contributing to the cold-pool propagation (Schumacher and Johnson, 2008). An inverse flow to the windward side is clearly shown in Fig. 9b (85–90 km of C–C'). Eventually, through vertical cross-sectional analysis, we highlight the cold pool and the downward flow as the important factors in explaining the sustainable convergence zone.

To describe CP, we introduced the three processes of (i) roughness change, (ii) cold pool and (iii) downward flow to help cold-pool propagation. The three elements interact with each other and exert a substantial effect in the presence of surface discontinuity. If there is no surface change, then the interaction among the elements is reduced and the convergence is not maintained. The low-level convergence due to roughness change affected the development of convection, and a cold pool, which occurs easily over dry land (Gentine et al., 2016), could well form under the developed precipitation system. For this reason, the convergence zone near the shoreline was sustained, and air that had been cooled sufficiently over the land by evaporation could propagate offshore.

The sensitivity for the surface was assessed by comparing the CTL and NL experiments. Figure 10 shows the spatial variation of prognostic variables simulated in each experiment for nine hours. For θ', the NL results were lower than the CTL ones, and the difference was more pronounced (> 0.4 K) over the land. Compared with the NL results, the CTL ones showed greater vertical velocity and TKE near the shoreline. Regarding vertical velocity, CTL was higher than NL, but over the land the downward flow of the convective system made the velocity lower (more negative). The TKE, which indicates the mixing of air, was obviously large in CTL. All three prognostic variables offer a spatial description of the aforementioned physical processes and indicate directly the effect of surface discontinuity.

3.4. *Quantification of coastal enhancement*

In some cases, the convective systems that develop in coastal regions cause much precipitation, but not always. This is because the systems do not always develop via surface discontinuity. For a convective system to develop and persist in a coastal region, the aforementioned elements

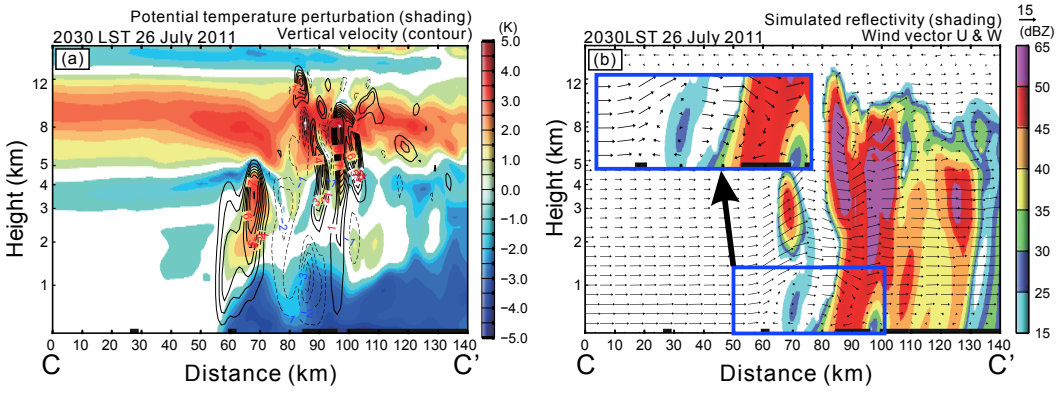

Fig. 9. Vertical cross-sections of (a) potential temperature perturbation (shading) and vertical velocity (contours), and (b) simulated radar reflectivity (shading) and wind vector (***U*** and ***W***) along the line depicted in Fig. 8.

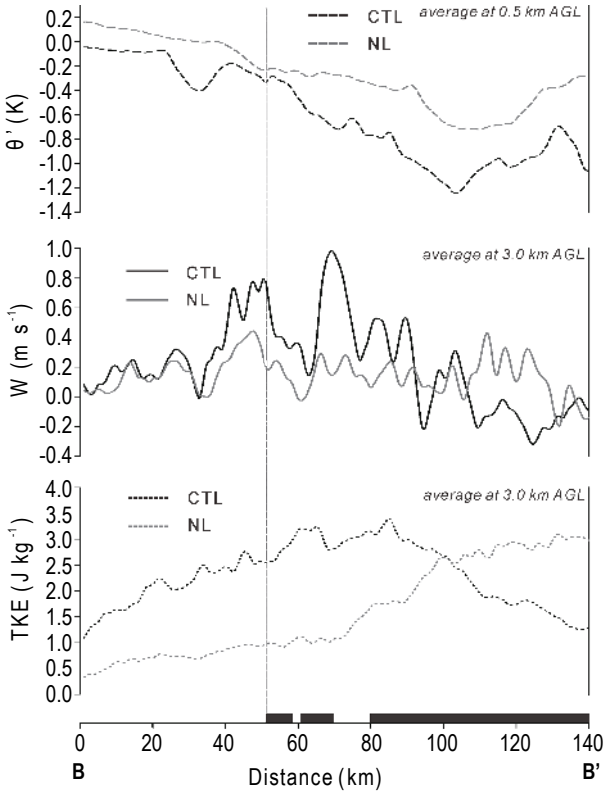

Fig. 10. Spatial variations of prognostic variables (θ', W and TKE) along transect B–B'. The black and grey lines indicate CTL and NL results, respectively. The horizontal black bars indicate onshore region. The plots show the time average for nine hours (1500 LST 26 to 0000 LST 27 July 2011).

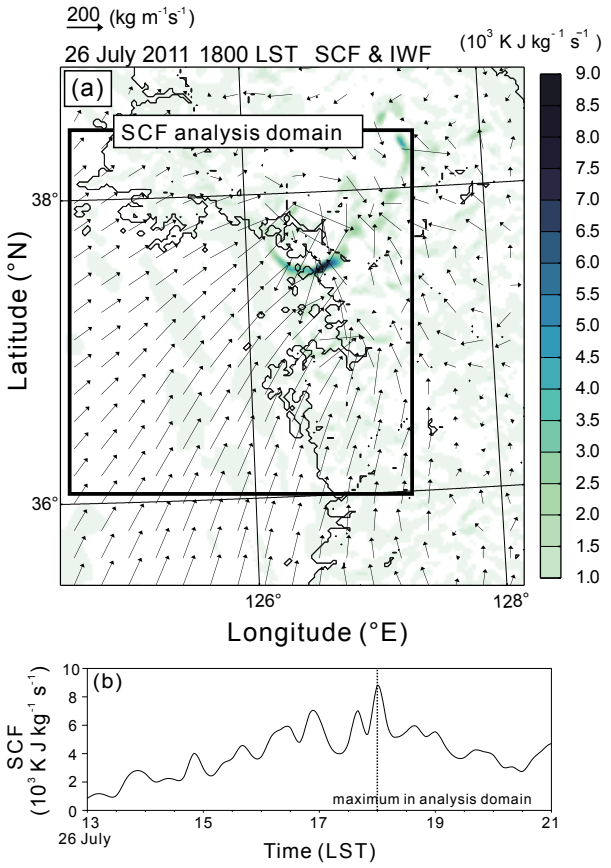

Fig. 11. (a) Spatiotemporal distribution of SCF (shading) and IWF (vectors) at 1800 LST 26 July 2011. (b) Time series of maximum SCF in the analysis domain. The dashed line indicates the time of Fig. 11a.

must be induced. Even though the interaction process is clear, the priority of the elements is not easy to discern; therefore, predictors may have difficulty in diagnosing or predicting the development of CP. Therefore, in the present study, we constructed the SCF using the analyzed variables (θ and TKE) that are fundamentally related to the CP development processes to express it as one quantified value [Eq. (2)]. To express the decreased wind and convergence, the airflow is represented by the difference term between the spatial mean ($\overline{V}$; within the SCF analysis domain) and given points ($\boldsymbol{V}$). Figure 11a shows the horizontal distributions of SCF and IWF when SCF is the highest (Fig. 11b). The southwestern IWF distribution indicates that the water vapor is inflowing strongly to the land from the sea, and its decrease over the land means that the physical processes mentioned above (roughness change, cold pool propagation, downward flow, and convection) acted as an obstacle that changed the vector. The potential convection energy identified by the long IWF vector is released by physical convection in the coastal area. As convection raises the low-level air, including a large amount of water vapor (q_v) to the upper layer, q_v is reduced because it condenses into raindrops at the convective condensation level, thereby causing the vector to be shorter at the surface. The directional change of the IWF vector is attributed to all the physical processes.

The shaded SCF that includes determinants for CP shows a remarkable distribution. The highest values of SCF were mainly inland, and the maximum value (>8 × 10^3 K J kg^{-1} s^{-1}) in the spatiotemporal range was found in the coastal region. The maximum SCF within the two-dimensional analysis domain varied with time (Fig. 11b), but the highest value occurred in the coastal region at 1800 LST, when the highest rainfall intensity happening in the surrounding area. This indicates that the SCF is sufficient for representing and diagnosing the development of CP.

4. Summary and conclusion

The purpose of this study was to improve the understanding of the CP at the western coast of Korea. Many mesoscale convective systems develop from the Yellow Sea because of surface discontinuity, and thermal differences between sea and land have been cited as the main causes of this discontinuity. However, as well as the thermal cause, this study suggests that a steep gradient of wind stress and θ can be major factors in the formation of the discontinuity, and that a well-formed cold pool and downward flow are responsible for maintaining the convergence zone.

Three-dimensional wind fields retrieved by Doppler radars revealed that a force acting in the opposite direction to that in which the system moved persisted at low levels.

The inland forcing was responsible for maintaining convection in the coastal region and the force formed along the coast. Several physical processes were taken as factors to explain the CP mechanism, and consequently it was analyzed and evaluated by simulation results.

First, surface-sensitivity experiments showed that this case was particularly sensitive to the surface conditions. The amount of rainfall differed considerably depending on the presence or absence of land cover, which validated the present study and provided it with direction. By analyzing the physical quantities of the model variables, we were able to assess which factors responded to the surface discontinuity and discuss their relevance.

The remarkably increased Reynolds stress provided evidence that a mechanical process (roughness) had a major influence on the decreased wind speed at the surface border. The stress increased as the roughness change spread to the upper layer, which eventually reduced the wind speed and convergence at the coast. The roughness change is a major element that can describe a stagnant precipitation system in the early stage of CP, but it cannot explain the maintenance of a system near the coast. The convergence zone was maintained and diffused around the coast, and the cold pool and downward flow were suggested as descriptors of its long-lasting. The reason why the convergence zone could continue is that deep evaporative cooling by the enhanced rainfall at the surface formed a cold pool, resulting in a steep gradient of potential temperature. The developed cold pool deepened the convective activity at its border. Evaporative cooling by raindrops occurs more easily on land than at the sea surface, making the gradient of the potential temperature near the shore steep. If the exchange of heat with the land is not significant, surface discontinuity provides a favorable condition for decreases in wind speed by roughness change, and maturity of the cold pool. The downward flow of the system also played an important role in maintaining and diffusing the convergence zone, as well as the cold pool toward the offshore. Eventually, not only the surface mechanical process of wind stress, but also the cold pool deepening inland and downward flows, had a profound effect on the formation and maintenance of the convergence zone, which led to concentrated precipitation in the coastal region. In particular, those steep gradients (wind stress and potential temperature) that contributed to the convergence were presented by the surface discontinuity and identified as a main element of CP.

We can extend the utility of the identified elements and mechanisms to estimate and forecast CP, and constructed the SCF for such a purpose. The vertically accumulated SCF of the indicated variables was sufficiently sensitive to the enhanced convection near the coast in both time and space and was therefore adequate for estimating CP.

This paper describes the mechanisms for CP, and the roughness effect has been studied. The force at the land discovered from radar wind fields was analyzed on the basis of model experiments. The identified elements for the force and CP were used to build the SCF index, which can quantify those processes. Although one case study cannot cover all CP mechanisms, the factors and their interactions shown herein will form the basis for understanding and predicting such mechanisms. Over-interpretation should be avoided because the SCF index was applied to one case only, and further studies are required to produce sufficient and meaningful verification results.

Acknowledgments. This research was funded by the Korea Meteorological Institute (Grant No. KMI 2018-05410).

REFERENCES

Attema, J. J., and G. Lenderink, 2014: The influence of the North Sea on coastal precipitation in the Netherlands in the present-day and future climate. *Climate Dyn.*, **42**(1–2), 505–519, https://doi.org/10.1007/s00382-013-1665-4.

Baidya Roy, S., and R. Avissar, 2002: Impact of land use/land cover change on regional hydrometeorology in Amazonia. *J. Geophys. Res.*, **107**(D20), 8037, https://doi.org/10.1029/2000JD000266.

Bergeron, T., 1949: The problem of artificial control of rainfall on the globe II. The coastal orographic maxima of precipitation in autumn and winter. *Tellus*, **1**(3), 15–32, https://doi.org/10.1111/j.2153-3490.1949.tb01264.x.

Braun, S. A., R. Rotunno, and J. B. Klemp, 1999: Effects of coastal orography on landfalling cold fronts. Part I: Dry, inviscid dynamics. *J. Atmos. Sci.*, **56**(4), 517–533, https://doi.org/10.1175/1520-0469(1999)056<0517:EOCOOL>2.0.CO;2.

Camberlin, P., and O. Planchon, 1997: Coastal precipitation regimes in Kenya. *Geografiska Annaler: Series A, Physical Geography*, **79**(1–2), 109–119, https://doi.org/10.1111/j.0435-3676.1997.00010.x.

Chen, G. X., X. Y. Zhu, W. M. Sha, T. Iwasaki, H. Seko, K. Saito, H. Iwai, and S. Ishii, 2015: Toward improved forecasts of sea-breeze horizontal convective rolls at super high resolutions. Part I: Configuration and verification of a Down-Scaling Simulation System (DS3). *Mon. Wea. Rev.*, **143**(5), 1849–1872, https://doi.org/10.1175/MWR-D-14-00212.1.

Christakos, K., G. Varlas, J. Reuder, P. Katsafados, and A. Papadopoulos, 2014: Analysis of a low-level coastal jet off the western coast of Norway. *Energy Procedia*, **53**, 162–172, https://doi.org/10.1016/j.egypro.2014.07.225.

Cressman, G. P., 1959: An operational objective analysis system. *Mon. Wea. Rev.*, **87**(10), 367–374, https://doi.org/10.1175/1520-0493(1959)087<0367:AOOAS>2.0.CO;2.

de Szoeke, S. P., E. D. Skyllingstad, P. Zuidema, and A. S. Chandra, 2017: Cold pools and their influence on the tropical marine boundary layer. *J. Atmos. Sci.*, **74**(4), 1149–1168, https://doi.org/10.1175/JAS-D-16-0264.1.

Drobinski, P., S. Bastin, T. Arsouze, K. Béranger, E. Flaounas, and M. Stéfanon, 2018: North-western Mediterranean sea-breeze circulation in a regional climate system model. *Climate Dyn.*, **51**, 1077–1093, https://doi.org/10.1007/s00382-017-3595-z.

Gentine, P., A. Garelli, S. B. Park, J. Nie, G. Torri, and Z. M. Kuang, 2016: Role of surface heat fluxes underneath cold pools. *Geophys. Res. Lett.*, **43**(2), 874–883, https://doi.org/10.1002/2015GL067262.

Gray, W. M., J. D. Sheaffer, C. W. Landsea, 1997: Climate trends associated with multidecadal variability of Atlantic hurricane activity. *Hurricanes*, 15–53, https://doi.org/10.1007/978-3-642-60672-4_2.

Gyakum, J. R., and R. E. Danielson, 2000: Analysis of meteorological precursors to ordinary and explosive cyclogenesis in the western North Pacific. *Mon. Wea. Rev.*, **128**(3), 851–863, https://doi.org/10.1175/1520-0493(2000)128<0851:AOMPTO>2.0.CO;2.

Hirata, H., R. Kawamura, M. Kato, and T. Shinoda, 2015: Influential role of moisture supply from the Kuroshio/Kuroshio Extension in the rapid development of an extratropical cyclone. *Mon. Wea. Rev.*, **143**(10), 4126–4144, https://doi.org/10.1175/MWR-D-15-0016.1.

Ikawa, M., and K. Saito, 1991: Description of a nonhydrostatic model developed at the Forecast Research Department of the MRI. Tech. Rep. MRI 28.

Jang, J., and S.-Y. Hong, 2014: Quantitative forecast experiment of a heavy rainfall event over Korea in a global model: Horizontal resolution versus lead time issues. *Meteor. Atmos. Phys.*, **124**(3–4), 113–127, https://doi.org/10.1007/s00703-014-0312-x.

Jang, M., C. H. You, J. B. Jee, S. H. Park, S. I. Kim, and Y. J. Choi, 2016: Three-dimensional analysis of heavy rainfall using KLAPS re-analysis data. *Atmosphere*, **26**(1), 97–109, https://doi.org/10.14191/Atmos.2016.26.1.097.

Jeong, J. H., D. I. Lee, and C. C. Wang, 2016: Impact of the cold pool on mesoscale convective system-produced extreme rainfall over southeastern South Korea: 7 July 2009. *Mon. Wea. Rev.*, **144**(10), 3985–4006, https://doi.org/10.1175/MWR-D-16-0131.1.

Ke, C.-Y., K.-S. Chung, T.-C. Chen Wang, and Y.-C. Liou, 2019: Analysis of heavy rainfall and barrier-jet evolution during Mei-Yu season using multiple Doppler radar retrievals: A case study on 11 June 2012. *Tellus A: Dynamic Meteorology and Oceanography*, **71**(1), 1–21, https://doi.org/10.1080/16000870.2019.1571369.

Langland, R. H., R. L. Elsberry, and R. M. Errico, 1995: Evaluation of physical processes in an idealized extratropical cyclone using adjoint sensitivity. *Quart. J. Roy. Meteor. Soc.*, **121**(526), 1349–1386, https://doi.org/10.1002/qj.49712152608.

Lee, D. K., H. R. Kim, and S. Y. Hong, 1998: Heavy rainfall over Korea during 1980–1990. *Korean Journal of the Atmospheric Sciences*, **1**(1), 523–547.

Lee, J. H., 2015: Turbulent boundary layer flow with a step change from smooth to rough surface. *International Journal of Heat and Fluid Flow*, **54**, 39–54, https://doi.org/10.1016/j.ijheatfluidflow.2015.05.001.

Lee, J. T., D. I. Lee, C.-H. You, H. Uyeda, Y.-C. Liou, and I.-S. Han, 2014: Dual-Doppler radar analysis of a near-shore line-shaped convective system on 27 July 2011, Korea: A case study. *Tellus A: Dynamic Meteorology and Oceanography*, **66**(1), 23453, https://doi.org/10.3402/tellusa.v66.23453.

Lee, J.-Y., W. Kim, and T.-Y. Lee, 2017: Physical and dynamic factors that drove the heavy rainfall event over the middle Korean Peninsula on 26–27 July 2011. *Asia-Pacific Journal of Atmospheric Sciences*, **53**(1), 101–120, https://doi.org/10.1007/s13143-017-0009-4.

Li, Y. P., and R. E. Carbone, 2015: Offshore propagation of coastal precipitation. *J. Atmos. Sci.*, **72**(12), 4553–4568, https://doi.org/10.1175/JAS-D-15-0104.1.

Lin, Y.-L., R. D. Farley, and H. D. Orville, 1983: Bulk parameterization of the snow field in a cloud model. *J. Climate Appl. Meteor.*, **22**(6), 1065–1092, https://doi.org/10.1175/1520-0450(1983)022<1065:BPOTSF>2.0.CO;2.

Liou, Y.-C., and Y.-J. Chang, 2009: A variational multiple-Doppler radar three-dimensional wind synthesis method and its impacts on thermodynamic retrieval. *Mon. Wea. Rev.*, **137**(11), 3992–4010, https://doi.org/10.1175/2009MWR2980.1.

Liou, Y.-C., S.-F. Chang, and J. Z. Sun, 2012: An application of the immersed boundary method for recovering the three-dimensional wind fields over complex terrain using multiple-Doppler radar data. *Mon. Wea. Rev.*, **140**(5), 1603–1619, https://doi.org/10.1175/MWR-D-11-00151.1.

Louis, J. F., M. Tiedtke, and J. F. Geleyn, 1982: A short history of the operational PBL-parameterization at ECMWF. *Proc. Workshop on Planetary Boundary Layer Parameterization*, Berkshire, UK, European Centre for Medium Range Weather Forecasts.

Mazón, J., and D. Pino, 2013: The role of sea-land air thermal difference, shape of the coastline and sea surface temperature in the nocturnal offshore convection. *Tellus A: Dynamic Meteorology and Oceanography*, **65**(1), 20027, https://doi.org/10.3402/tellusa.v65i0.20027.

Murakami, M., T. L. Clark, and W. D. Hall, 1994: Numerical simulations of convective snow clouds over the sea of Japan. *J. Meteor. Soc. Japan*, **72**(1), 43–62, https://doi.org/10.2151/jmsj1965.72.1_43.

Nyberg, A., and H. Modén, 1966: The seasonal distribution of precipitation in the area east of Stockholm and the daily distribution in a few selected cases. *Tellus*, **18**(4), 745–750, https://doi.org/10.1111/j.2153-3490.1966.tb00295.x.

Oerlemans, J., 1980: A case study of a subsynoptic disturbance in a polar outbreak. *Quart. J. Roy. Meteor. Soc.*, **106**(448), 313–325, https://doi.org/10.1002/qj.49710644806.

Persson, P. O. G., P. J. Neiman, B. Walter, J.-W. Bao, and F. M. Ralph, 2005: Contributions from California coastal-zone surface fluxes to heavy coastal precipitation: A CALJET case study during the strong El Niño of 1998. *Mon. Wea. Rev.*, **133**(5), 1175–1198, https://doi.org/10.1175/MWR2910.1.

Pielke Sr, R. A., J. Adegoke, A. BeltraáN-Przekurat, C. A. Hiemstra, J. Lin, U. S. Nair, D. Niyogi, and T. E. Nobis, 2007: An overview of regional land-use and land-cover impacts on rainfall. *Tellus B: Chemical and Physical Meteorology*, **59**(3), 587–601, https://doi.org/10.1111/j.1600-0889.2007.00251.x.

Pires, L. B. M., G. Fisch, R. Gielow, L. F. Souza, A. C. Avelar, I. B. de Paula, and R. da Mota Girardi, 2015: A study of the internal boundary layer generated at the Alcantara Space Center. *American Journal of Environmental Engineering*, **5**(1A), 52–64, https://doi.org/10.5923/s.ajee.201501.08.

Plant, R. S., and B. W. Atkinson, 2002: Sea-breeze modification of the growth of a marine internal boundary layer. *Bound.-Layer Meteor.*, **104**(2), 201–228, https://doi.org/10.1023/A:1016045229957.

Prandtl, L., 1925: Bericht uber Untersuchungen zur ausgebildeten Turbulenz. *Zeitschrift Für angewandte Mathematik und Mechanik*, **5**(1), 136–139.

Ross, A. N., A. M. Tompkins, and D. J. Parker, 2004: Simple models of the role of surface fluxes in convective cold pool evolution. *J. Atmos. Sci.*, **61**(13), 1582–1595, https://doi.org/10.1175/1520-0469(2004)061<1582:SMOTRO>2.0.CO;2.

Roxy, M. K., K. Ritika, P. Terray, R. Murtugudde, K. Ashok, and B. N. Goswami, 2015: Drying of Indian subcontinent by rap-

id Indian Ocean warming and a weakening land-sea thermal gradient. *Nature Communications*, **6**, 7423, https://doi.org/10.1038/ncomms8423.

Schlemmer, L., and C. Hohenegger, 2016: Modifications of the atmospheric moisture field as a result of cold-pool dynamics. *Quart. J. Roy. Meteor. Soc.*, **142**(694), 30–42, https://doi.org/10.1002/qj.2625.

Schumacher, R. S., and R. H. Johnson, 2008: Mesoscale processes contributing to extreme rainfall in a midlatitude warm-season flash flood. *Mon. Wea. Rev.*, **136**(10), 3964–3986, https://doi.org/10.1175/2008MWR2471.1.

Segami, A., K. Kurihara, H. Nakamura, M. Ueno, and I. Takano, 1989: Description of Japan spectral model. JMA/NPD Tech. Rep. 25, 41 pp.

Smith, W. H. F., and P. Wessel, 1990: Gridding with continuous curvature splines in tension. *Geophysics*, **55**(3), 293–305, https://doi.org/10.1190/1.1442837.

Sridhar, V., 2013: Tracking the influence of irrigation on land surface fluxes and boundary layer climatology. *J. Contemp. Water Res. Educ.*, **152**(1), 79–93, https://doi.org/10.1111/j.1936-704X.2013.03170.x.

Sun, J. H., and T.-Y. Lee, 2002: A numerical study of an intense quasi-stationary convection band over the Korean Peninsula. *J. Meteor. Soc. Japan*, **80**(5), 1221–1245, https://doi.org/10.2151/jmsj.80.1221.

Tseng, Y.-H., and J. H. Ferziger, 2003: A ghost-cell immersed boundary method for flow in complex geometry. *J. Comput. Phys.*, **192**(2), 593–623, https://doi.org/10.1016/j.jcp.2003.07.024.

Tsuboki, K., A. Sakakibara, 2002: Large-scale parallel computing of cloud resolving storm simulator. *Int. Symp. High Perform. Comp.*, 243–259, https://doi.org/10.1007/3-540-47847-7_21.

Woodruff, J. D., J. L. Irish, S. J. Camargo, 2013: Coastal flooding by tropical cyclones and sea-level rise. *Nature*, **504**(7478), 44–52, https://doi.org/10.1038/nature12855.

Wu, J., 1969: Wind stress and surface roughness at air-sea interface. *J. Geophys. Res.*, **74**(2), 444–455, https://doi.org/10.1029/JB074i002p00444.

Wu, J., 1982: Wind-stress coefficients over sea surface from breeze to hurricane. *J. Geophys. Res.*, **87**(C12), 9704–9706, https://doi.org/10.1029/JC087iC12p09704.

Yang, L. B., G. Q. Sun, L. Zhi, and J. J. Zhao, 2018: Negative soil moisture-precipitation feedback in dry and wet regions. *Scientific Reports*, **8**(1), 4026, https://doi.org/10.1038/s41598-018-22394-7.

Zhang, J., S. Wang, and B. Clarke, 2004: WSR-88D reflectivity quality control using horizontal and vertical reflectivity structure. Preprints, *11th Conf. on Aviation, Range and Aerospace Meteorology*, Hyannis, MA, Amer. Meteor. Soc., 5 pp.